Protein Response to Photodissociation of CO from Carbonmonoxymyoglobin Probed by Time-Resolved Infrared Spectroscopy of the Amide I Band†

Timothy P. Causgrove and R. Brian Dyer*

Division of Chemical and Laser Sciences (Mail Stop J567), Los Alamos National Laboratory, Los Alamos, New Mexico 87545

Received April 26, 1993; Revised Manuscript Received September 9, 1993®

ABSTRACT: Protein conformational changes coupled to the ligation reactions of carbon monoxide in myoglobin (Mb) are detected by time-resolved infrared spectroscopy. An apparatus based on a tunable diode laser operating in the region of 1650 cm^{-1} is used to probe changes in the amide I absorption band of the protein in response to photodissociation and subsequent rebinding of CO. The time course of changes in the amide I band is shown to follow the recombination of photolyzed CO with Mb. A time-resolved difference spectrum in the amide I region is generated by tuning the diode laser probe source. The features in the IR difference spectrum are assigned to the motions of the polypeptide backbone associated with the global relaxation of the protein from the ligated to the deoxy conformation. A static difference spectrum generated by subtracting FTIR spectra of carbonmonoxy-Mb and deoxy-Mb is essentially identical to the transient spectrum, indicating that the protein relaxation is complete with the 100-ns time resolution of the experiment.

A critical feature of the biological function of heme proteins such as hemoglobin and myoglobin is the direct coupling of protein motion to the process of binding exogenous ligands to the heme. There are at least two ways in which conformational changes of the protein play a role in the ligation reactions. A substantial, specific conformational relaxation is associated with the transition from the ligated to the unligated form of the protein. In MbCO,[1] for example, upon loss of CO the Fe moves 0.4 Å out of the plane of the heme, there is a coupled displacement of the proximal helices, and the heme pocket contracts (Kuriyan et al., 1986). The analogous tertiary structural changes of the monomer heme subunits of hemoglobin ultimately lead to the R → T quaternary structural transition, the allosteric control mechanism of O_2 binding efficiency (Perutz et al., 1987). Second, on the basis of the X-ray crystal structures of Mb and MbCO (Kuriyan et al., 1986; Takano, 1977) it has long been recognized that the movement of ligands from the heme pocket to the solvent requires the development of transient pathways (Nobbs, 1966). Consequently, the rate of ligand diffusion to and from the binding site is determined in part by the protein motion. The diffusion of the ligand through the protein may involve the formation of specific pathways through the protein which are gated by specific structural changes, or at the other extreme, the ligand may diffuse through the protein in a process controlled by random fluctuations of the protein structure.

The nature of the protein motion coupled to protein function has been the subject of intense theoretical and experimental investigation. Frauenfelder and co-workers have developed a phenomenological model in which proteins assume a large number of nearly isoenergetic conformations (conformational substates) (Frauenfelder et al., 1991). Protein motion dynamically samples the distribution of conformational substates, the dwell time in each depending on the barriers separating conformations. The distribution of substates and energy barriers leads to highly nonexponential protein relaxation which is reflected in ligand rebinding kinetics at low temperatures or high solvent viscosity. Another view of protein motion has been suggested by Miller, in which the protein responds as a rigid body, producing a collective displacement of a large number of atoms in response to ligand dissociation (Richard et al., 1992). This model is based on picosecond phase grating experiments which suggest that the global structural relaxation of Hb and Mb does not sample intermediates, but instead occurs in phase with the optical trigger, on the time scale of the out-of-plane motion of the proximal histidine. This model does not rule out the possibility of conformational substates playing a role in slower relaxation processes, for example, those coupled to ligand motion through the protein. A number of theoretical approaches have provided additional insight into the coupling of protein and ligand motion. Ligand trajectories through the protein have been simulated in molecular dynamics calculations which incorporate the molecular details of the Mb structure to determine the predominant ligand pathways (Case & Karplus, 1979; Elber & Karplus, 1990). These approaches provide a clear connection between protein dynamics and function, but have until recently been difficult to test experimentally.

Most of our understanding of the ligand-binding processes of Hb and Mb is the result of studies of the photodissociation of ligands from the heme-binding site, pioneered by Gibson (1956). Photochemical triggering of the reaction prepares a well-defined initial state which allows the investigation of the fundamental steps of ligand escape from the heme pocket and ligand recombination and the protein motions coupled to these processes. CO ligation is generally preferred in time-resolved spectroscopic studies due to the stability of MbCO in solution and because CO exhibits almost unit quantum efficiency for photodissociation and little geminate recombination (Gibson et al., 1986; Henry et al., 1983). Photolysis of CO from Mb and its recombination processes have been studied by a large array of spectroscopic techniques, including UV-vis absorption (Ansari et al., 1992; Henry et al., 1983; Martin et al., 1983), EXAFS (Powers et al., 1987), time-resolved circular dichroism (Xie & Simon, 1991), time-resolved infrared (TRIR) (Dixon et al., 1988; Gerwert et al., 1985; Jedju et al., 1988), and time-resolved resonance Raman (Findsen et al., 1985). These studies have focused on the ligand or the heme; information

† This work was supported by NIH Grant GM 45807.

* Author to whom correspondence should be addressed.

® Abstract published in *Advance ACS Abstracts,* October 15, 1993.

[1] Abbreviations: Mb, myoglobin; MbCO, carbonmonoxymyoglobin; Hb, hemoglobin; IR, infrared; FTIR, Fourier transform infrared; TRIR, time-resolved infrared; YAG, yttrium–aluminum–garnet.

0006-2960/93/0432-11985$04.00/0

on the protein itself is indirectly inferred from these measurements.

It has long been known that infrared spectra in the amide region are sensitive to protein secondary structure (Elliott & Ambrose, 1950). Recent advances in equipment and techniques have permitted researchers to quantitatively predict secondary structures from infrared spectra (Dong et al., 1990, 1992; Dousseau & Pézolet, 1990; Kaiden et al., 1987; Susi & Byler, 1986), particularly in the amide I region (Dong et al., 1990, 1992; Dousseau & Pézolet, 1990). Furthermore, developments in the field of TRIR spectroscopy in our laboratories and others make it possible to probe infrared changes in the amide I spectral region from hundreds of femtoseconds to seconds (Causgrove & Dyer, 1993a; Diller et al., 1991). The IR changes track molecular dynamics down to ultrashort time scales because vibrational transitions respond to changes in structure in times as short as the periods of the vibrations themselves. The structural specificity and time resolution of this approach make it possible to study protein functional dynamics on all relevant time scales. In addition, TRIR spectroscopy is uniquely suited to study protein motions with minimal interference from the heme, in contrast to techniques based on visible light such as resonance Raman and circular dichroism. The use of time-resolved difference spectra in the amide I region provides a powerful tool for the study of the protein dynamics which are coupled to (triggered by) the ligation (or photodissociation) of small molecules to (from) the heme.

TRIR spectroscopy has already played a large role in investigating the ligand-binding dynamics in Mb and Hb from the subpicosecond (Anfinrud et al., 1989; Jedju et al., 1988) to the millisecond time scale (Dixon et al., 1988; Gerwert et al., 1985). These studies probed the Fe–CO bleach at 1943 cm^{-1} and in some cases, the 2135 cm^{-1} (Mb) or 2100 cm^{-1} (Hb) absorption of photolyzed CO trapped in the heme pocket. Herein we report the use of TRIR spectroscopy in the amide I region to directly probe the protein dynamics coupled to the photodissociation and recombination of CO in Mb.

MATERIALS AND METHODS

The time-resolved infrared absorption apparatus has been described previously (Dyer et al., 1989) and is based on a frequency-doubled, Q-switched Nd:YAG pump laser (532 nm, 7-ns pulse width) and a CW lead salt diode infrared probe laser. The pump laser initiates the IR transient (e.g., CO photolysis), and the transient absorbance of the single-wavelength CW infrared probe laser is monitored in real time with a fast rise time semiconductor infrared detector. The infrared probe laser is tuned to obtain the kinetic response at different wavelengths or the infrared spectrum at a specific time delay after the pump pulse. The following modifications were made to our apparatus to permit operation in the amide I spectral region. A HgCdTe detector having a peak sensitivity in the 6–10-μm spectral region is used instead of the InSb detector, which is insensitive in the amide I spectral region. The biased preamplifier has a bandwidth of DC to 20 MHz, yielding a detector–amplifier rise time (10–90% of full-scale deflection) of 300 ns. The instrument response and the zero of time are determined experimentally by generating an infrared transient known to have an instantaneous rise time on this time scale [the Fe–CO bleach of MbCO is generally employed since it occurs on a subpicosecond time scale (Anfinrud et al., 1989; Moore et al., 1987)]. This experimentally determined instrument response is then convolved with a single exponential to best fit the rise of an infrared

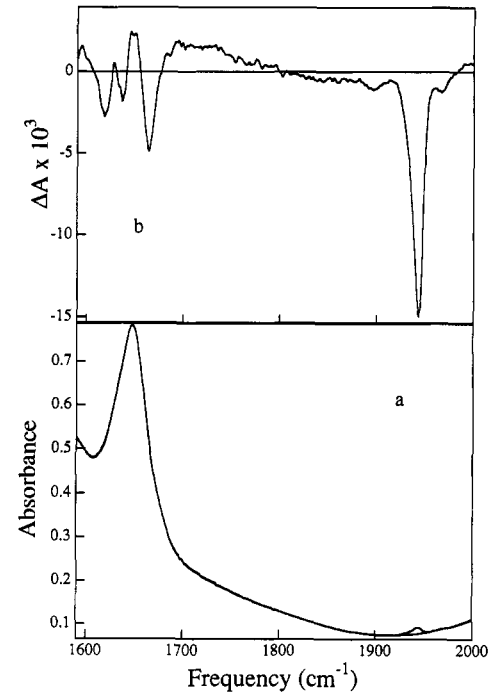

FIGURE 1: Static FTIR spectra of 1.3 mM horse skeletal muscle Mb in the amide I and CO region: (a) overlay of the deoxy and carbonmonoxy spectra (the CO peak is barely visible at 1943 cm^{-1}); (b) difference spectrum (Mb – MbCO).

transient. The laser diode used as a probe source in the amide I region is temperature tunable between 1605 and 1725 cm^{-1} with a mode spacing of about 4.5 cm^{-1}. Each mode is tunable by about 1 cm^{-1}, leaving small gaps inaccessible to the probe source. A second diode tunable in the 5-μm region is used to monitor the CO stretching frequency. The two diodes are contained in a liquid nitrogen dewar which can be translated to interchange them without modification of the optical alignment. The amide I and CO transient absorptions are monitored under identical conditions using this arrangement. Transients are typically obtained using pulse energies of 120 μJ in a 2-mm-diameter spot. Multiple transients are averaged at the laser repetition rate of 10 Hz. The measured decay is generated by subtracting traces taken with the Nd:YAG laser blocked from those with the laser unblocked to remove noise caused by diode laser fluctuations and detector pickup of electronic noise.

Carbonmonoxymyoglobin (MbCO) was prepared by dissolving lyophilized sperm whale myoglobin (Sigma) or horse skeletal muscle myoglobin (Sigma) in 50 mM phosphate buffer, pD 7.4 (in D_2O). The heme was reduced with 5 mM sodium dithionite and liganded with CO by several cycles of degassing and back-filling with CO. Final samples were 0.8–2.0 mM MbCO held in 50-μm sealed cells with CaF_2 windows. Sample integrity and complete CO ligation were checked by obtaining the UV-vis spectra on a CARY 17 spectrophotometer. FTIR spectra of the samples were taken on a Bio-Rad (Digilab) FTS 896. The measured intensity of the Fe–CO absorption was in agreement with the previously reported extinction coefficient for this absorption (Dixon et al., 1988).

RESULTS

The static FTIR spectra of identical, reduced horse skeletal muscle Mb samples in D_2O with and without added CO are overlaid in Figure 1a. The only obvious difference between these spectra is the band at 1943 cm^{-1}, due to the bound CO stretch (Fe–CO). When these spectra are subtracted, however,

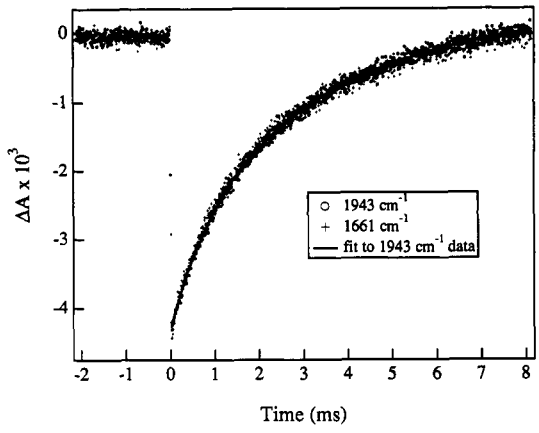

FIGURE 2: Time-resolved IR absorption traces of 0.8 mM MbCO at 1943 and 1662 cm^{-1}. The data have peak absorbance changes of 4.3×10^{-3} and 1.6×10^{-3}, respectively; the 1662 cm^{-1} trace has been scaled for comparison. Each of the decay traces is an average of data from 1600 individual laser shots. The solid line is a three-parameter fit to the 1943 cm^{-1} data according to A+B second-order kinetics (see text).

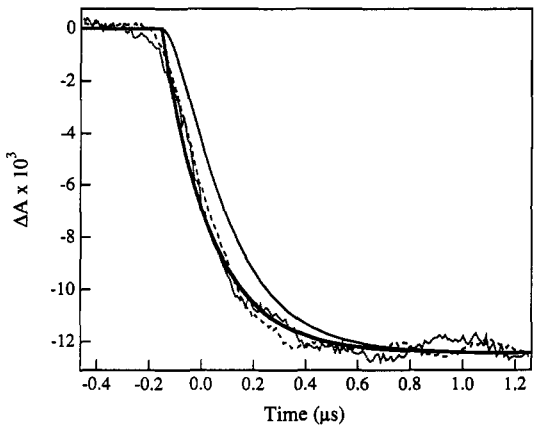

FIGURE 3: Time-resolved IR absorption traces of MbCO at 1943 (···) and 1666 cm^{-1} (- - -) collected on a fast time scale in order to resolve the rise of the transients. The leftmost solid trace is a fit of the instantaneous instrument response to a single exponential (τ = 230 ns); the rightmost solid trace is a convolution of the instantaneous instrument response with a 100-ns exponential rise.

the difference spectrum (Figure 1b) reveals features in the amide I band which result from the difference in conformation between the deoxy and carbon monoxy forms of the protein. These features represent a small fraction ($<10^{-2}$) of the total intensity of the amide I absorption. This difference spectrum is comparable to the steady-state redox FTIR difference spectrum (reduced minus oxidized) of horse Mb which has recently been generated using a novel electrochemical cell (Schlereth & Mäntele, 1992). The latter difference spectrum is expected to be somewhat similar to the spectrum in Figure 1 because both oxidation and ligation of deoxymyoglobin result in a shortening of Fe–N bonds, movement of the iron atom toward the ring plane, and a concomitant movement of the F helix toward the heme. Indeed, there are many similarities between the data, including the peaks near 1646 and 1664 cm^{-1} and the minor peaks at 1677 and 1695 cm^{-1}. The differences in the spectra are primarily at the low-frequency side of amide I.

Typical TRIR absorption changes following photodissociation of CO at 1943 cm^{-1} (Fe–CO band) and at 1662 cm^{-1} (amide I band) are shown in Figure 2. The traces were taken under identical conditions (i.e., using the same amplifiers, HgCdTe detector, and excitation energy). They have been normalized to the same peak amplitude for comparison of the rate of recovery of the two signals. Although the signal at 1662 cm^{-1} is smaller, the signal-to-noise ratios are similar due to greater laser power from the lower frequency diode as well as higher responsivity of the detector at this wavelength. Analysis of the traces was done using the so-called A+B second-order kinetics, fitting the data to the equation

$$\Delta A = \frac{\epsilon l[\mathrm{Mb}]\left(1 - \frac{[\mathrm{Mb}]}{[\mathrm{CO}]}\right)}{\exp(kt([\mathrm{CO}] - [\mathrm{Mb}])) - \frac{[\mathrm{Mb}]}{[\mathrm{CO}]}} + b$$

where [Mb] is the concentration of unliganded Mb immediately after the flash, [CO] is the initial concentration of free CO, and k is the second-order rate constant. The initial concentration of CO was taken as [Mb] + 0.8 mM, the concentration of saturated CO solution at 7500 ft above sea level. The second-order rate constant was a variable in the fitting, and the extinction coefficient of the Fe–CO absorption at 1943 cm^{-1}, ϵ, was fixed at 1920 M^{-1} cm^{-1} as determined by Dixon et al. (1988). The path length, l, was fixed at 50 μm. The additional parameter b was required due to a small baseline offset. The resulting fits gave second-order rate constants of 3.8×10^5 (1943 cm^{-1}) and 4.1×10^5 M^{-1} s^{-1} (1662 cm^{-1}), within experimental error of each other, but slightly lower than the value of 5.0×10^5 M^{-1} s^{-1} determined by UV-vis spectroscopy (Gibson et al., 1986), possibly due to the higher protein concentration used in the TRIR experiments. The best fit at 1943 cm^{-1} was obtained with an initial concentration of unliganded myoglobin of 0.46 mM, corresponding to ~60% photolysis. For fitting of data acquired at 1662 cm^{-1}, [Mb] was fixed at 0.46 mM and the extinction coefficient determined by fitting was 693 M^{-1} cm^{-1}. Errors may be introduced in this analysis by the assumption of a saturated CO solution or by slightly different photolysis efficiencies between the two measurements.

Transients were also taken at several wavelengths using a faster amplifier in an attempt to resolve kinetics due to the motion of the protein. The rise time of the 1662 cm^{-1} amide I transient is compared to that of the Fe–CO bleach at 1943 cm^{-1} in Figure 3. The CO bleach occurs faster than 300 fs (Anfinrud et al., 1989; Jedju et al., 1988) and therefore represents the response time of our instrument. The experimentally determined instrument response convolved with a 100-ns exponential function is also shown in Figure 3. This convolution indicates that the signal-to-noise of our data would allow a rate of 100 ns to be resolved. The growth of the 1662 cm^{-1} transient is clearly faster than 100 ns. In addition to the 1662 cm^{-1} trace shown in Figure 3, the initial rise was obtained at 1619, 1647, and 1676 cm^{-1} (all of the major difference features). In all cases, the rise in the absorption change is faster than 100 ns.

By tuning the frequency of the probe source, transients such as those shown in Figure 2 were generated across the amide I band from 1608 cm^{-1} to 1723 cm^{-1}. The initial amplitude of each of these transients was recorded and plotted against frequency to create a Mb – MbCO difference spectrum for sperm whale myoglobin (Figure 4a) with a time resolution of approximately 1 μs. The spectrum contains several features, the most prominent of which is peaked at 1664 cm^{-1} with an absorbance change of 1.4×10^{-3} (using 1.6 mM MbCO), compared to an absorbance of 0.8 for the total amide I peak. The spectrum shows several other features, all of which are reproducible. The width of most peaks in the difference spectrum appears to be about 8–10 cm^{-1}. The TRIR difference

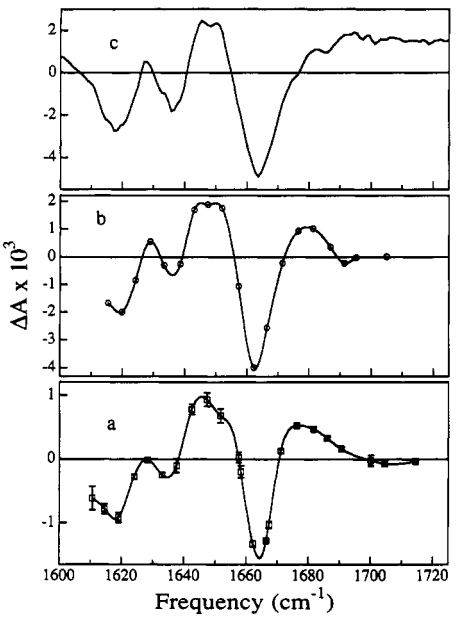

FIGURE 4: (a) TRIR difference spectrum of 1.6 mM Mb from sperm whale, generated from initial amplitudes of IR transients in the amide I region. Squares are the actual data (error bars show the standard deviation of the data); the solid line is a cubic spline interpolation. (b) TRIR difference spectrum using 4 mM horse skeletal muscle Mb. (c) Static difference spectrum (Mb – MbCO) generated from FTIR spectra of MbCO and deoxy-Mb samples of 1.3 mM horse skeletal muscle Mb.

spectrum was also obtained for horse skeletal muscle Mb (Figure 4b), which has an amino acid sequence slightly different from that of sperm whale Mb. The largest difference between the two samples is in the high-frequency region, where horse Mb shows a sharper 1680 cm^{-1} peak than sperm whale myoglobin with no signals observable in the 1700–1720 cm^{-1} range. Figure 4c shows the *static* difference spectrum generated by subtraction of the FTIR spectrum of deoxy-Mb from the FTIR spectrum of MbCO for horse skeletal muscle Mb. Although the Fe–CO bleach is not shown in these spectra, the ratio of the peak intensity at 1943 cm^{-1} to that at 1664 cm^{-1} is approximately 3:1 in both the static and the time-resolved experiments. This static spectrum is essentially identical to the transient spectrum, except in the region above 1690 cm^{-1}, due to a baseline subtraction problem. This baseline problem illustrates some of the advantages of the TRIR approach; many of the difficulties associated with steady-state FTIR spectra are avoided since explicit subtraction of protein, water, and water vapor backgrounds is unnecessary.

One potential complication of these TRIR experiments is the possibility of the pump pulse producing thermal artifacts due to the heating of the heme and subsequent heating of the protein and surrounding solvent. The possibility of artifacts due to heating of the protein was tested using deoxymyoglobin as a control. With the excitation conditions employed, no observable transients in the amide I region were produced in the deoxy-Mb sample (in other words, the photoexcited spectrum of deoxy-Mb is identical to the unexcited deoxy-Mb spectrum in the amide I region). The possibility of artifacts due to heating of the solvent was tested by obtaining static FTIR spectra of D_2O as a function of temperature. The D_2O background is featureless in the region from 1600 to 1700 cm^{-1} and shows a uniform decrease in absorbance with increasing temperature. The absorbance decrease is linear with temperature over the range from 4 to 40 °C with a slope that is essentially constant over this spectral region and equals 3×10^{-3} AU/°C. If we assume that all of the energy absorbed in our experiments ($\sim 20\ \mu J$) is converted to heat, we calculate a temperature rise of 0.03 °C in the absorbing volume. This ΔT should result in a constant decrease in the D_2O background absorbance of $\sim 1 \times 10^{-4}$ AU, which is the magnitude of the noise in our experiments. When an observable thermal artifact is deliberately produced by a 5-fold increase in the pump power, it appears as a bleach with a magnitude independent of wavelength and with a lifetime of several milliseconds. Cooling of the irradiated volume, determined by the rate of heat flow into the bulk, is independent of and substantially slower than the heme–CO recombination kinetics. In contrast, the recovery of the amide I transients precisely tracks the heme–CO recombination rate as seen in Figure 2. These control studies provide conclusive evidence that the observed amide I transients are free from thermal artifacts.

DISCUSSION

The features observed in the static FTIR difference spectrum are due to the static structural differences between the carbon monoxy and deoxy forms of Mb. These static structural differences have been well characterized in single crystals by X-ray diffraction (Kuriyan et al., 1986). The transition from the liganded form to the deoxy form causes two major structural changes. A global displacement of the protein atoms on the proximal side of the heme is coupled to the movement of the Fe atom 0.4 Å out of the heme plane and the concomitant displacement of the proximal histidine. It should be emphasized that this global motion is a displacement of the F and H helices and that the backbone *conformational* change is primarily localized in the corners to accommodate the helix movements. In addition, the heme pocket constricts in the absence of a bound ligand. The nature of this constriction is a localized rearrangement of side chains on the distal side of the heme, the largest motions involving the distal histidine (His64) and Arg45 side chains.

While the details of the structural differences between MbCO and deoxy-Mb are well understood, the dynamics of these changes are not. Furthermore, transient structures must be formed as intermediates which allow movement of the CO in and out of the heme pocket since no such pathways exist in the static structures of both MbCO and deoxy-Mb. The time-resolved infrared transients described here directly probe the dynamics of the protein response to CO photodissociation. Transients throughout the amide I band show instrument-limited rise times. Furthermore, the spectrum constructed from the initial amplitudes of such transients is identical to the static FTIR difference spectrum (Figure 4). The only difference between the transient and static spectra which is greater than the experimental uncertainty is in the region above 1690 cm^{-1}, which is due to a baseline subtraction problem in the FTIR difference spectrum. We conclude that the protein motion associated with ligand photodissociation, or at least the portion observable in the amide I IR band, is complete within 100 ns. In addition, the decays of the IR transients throughout the amide I region exactly track the CO recombination dynamics measured at 1943 cm^{-1} as illustrated in Figure 2. As expected, the rate-limiting step for return to the MbCO conformation is clearly the rebinding of CO.

A more specific interpretation of these dynamics requires the assignment of the IR difference features to specific structural changes. The assignment of infrared band shapes and subbands from steady-state FTIR spectra to specific secondary structures is currently an active area in the literature. The main techniques for resolving subbands in the amide I

region have been resolution enhancement by Fourier self-deconvolution (Surewicz & Mantsch, 1988; Susi & Byler, 1986) and generation of second-derivative spectra (Dong et al., 1990, 1992). It has been noted (Surewicz et al., 1993) that both of these techniques require very high signal-to-noise and careful elimination of water vapor bands. Recently, criteria for the subtraction of water and water vapor backgrounds have been developed to allow consistent resolution of bands beneath the amide I envelope and assignment of these bands to specific secondary structures for both H_2O and D_2O solutions.

There are many complications in the comparison of these assignments to the features seen in Figure 4 and other difference spectra. First, the difference spectrum is the sum of all changes in the protein, which may involve a complex superposition of bands. Also, there may be contributions to Figure 4 from amino acid side chain vibrations, which are considered small when measuring the overall amide I spectrum. However, the difference spectrum is sensitive to only those vibrations that change, which may increase the relative contribution of specific side-chain vibrations. Another problem derives from the magnitude of changes seen in Figure 4. Comparison of the area of the overall amide I peak to that of the 1664 cm^{-1} bleach in Figure 4a (corrected for photolysis efficiency) gives a ratio of 300:1, corresponding to a bleach of less than one backbone CO vibration. In addition, the extinction coefficients of changes in the amide I region are generally smaller than those determined for single amino acid side chain vibrations in D_2O (Chirgadze et al., 1975). This leads us to conclude that the differences in Figure 4 are composed of bands which have shifted by a small amount compared to their width, rather than large shifts of relatively narrow bands.

The candidates most likely to contribute side-chain vibrations in the amide I region are the Arg45 and distal histidine residues. The distal histidine may contribute a weak side-chain vibration at 1604 cm^{-1} in the static FTIR difference spectrum, due to the imidazole ring-breathing mode. The intensity and frequency of this absorption are consistent with the spectrum observed for model imidazole compounds (Chirgadze et al., 1975). This assignment requires that this band be significantly shifted in the deoxy form; while this is possible given the substantial change in environment of the imidazole, this assignment remains speculative.

X-ray structures have shown that Arg45 forms a salt bridge with one of the propionate groups of the heme; this interaction is strongly perturbed by the binding of CO, which causes the Arg45 side chain to exist in at least two different conformations, one of which is significantly different from the deoxy conformation (Kuriyan et al., 1986). The latter conformation has been postulated (Kuriyan et al., 1986) to be related to the formation of a ligand pathway out of the protein because it allows the distal histidine to rotate out of the heme pocket. Further evidence for the possible role of Arg45 in the ligand entry and escape from the binding pocket comes from spectroscopic studies of Mb with mutations at position 45 (Lambright et al., 1989; Westrick et al., 1990). These results emphasize the importance of a direct spectroscopic handle for the Arg45 side chain.

Difference features due to Arg45 should appear around 1608 and 1586 cm^{-1}, as arginine itself has relatively intense ($\epsilon > 500$ M^{-1} cm^{-1}) peaks at these frequencies (Chirgadze et al., 1975). No difference features are observed at these frequencies in the static difference spectrum (Figure 1); these frequencies were not accessible with the diodes available and hence were not probed in transient experiments. The peak at 1707 cm^{-1} in both the static and the transient difference spectra of sperm whale Mb, however, may be influenced by changes in the Arg45 conformation. This band may arise from -COOX vibrations of Glu, Asp, or heme propionate groups; Schlereth and Mäntele (1992) speculated that features near 1680 and 1695 cm^{-1} arose from heme propionate vibrations. The perturbation of the Arg45 side-chain interaction with the heme proprionate group may result in the difference feature at 1707 cm^{-1}. It should be noted that the peak at 1707 cm^{-1} does not represent a difference between -COOX and -COO- states, as the observed peak is too small. The extinction coefficient determined from Figure 4a is only 44 M^{-1} cm^{-1} compared to a literature value of greater than 200 M^{-1} cm^{-1} (Chirgadze et al., 1975) for typical carboxylic vibrations. Therefore, this peak would more likely represent a shift due to a change in the interaction of this group with Arg45. Further evidence in support of this assignment of the 1707 cm^{-1} peak comes from comparison of the transient difference spectra of sperm whale and horse Mb in this region (Figure 4a,b). Horse Mb, which contains lysine rather than arginine at position 45, lacks the 1707 cm^{-1} peak.

Although side-chain vibrations may make a contribution to the difference spectra of Figure 4, the main difference features appear to be due to changes in the polypeptide backbone. These differences represent the perturbations of secondary conformation associated with the global motion of atoms on the proximal side of the heme. Correlations of amide I band frequencies with specific secondary structures have been made for proteins in H_2O solution (Dong et al., 1990) and for a standard protein set in D_2O (Susi & Byler, 1986). Although there is general agreement between the two assignments, there are some differences in the exact frequency assignments. The most straightforward assignment is that for α-helix, which shows only a single narrow band at 1653–1656 cm^{-1}. Mb, which is 80% α-helix, is dominated by a single peak at 1654 cm^{-1} (Dong et al., 1990). Interestingly, the difference spectra in Figure 4 have an isosbestic point near this frequency, suggesting that the secondary structure of the helices is relatively unperturbed between the two forms of the protein. The bleach at 1664 cm^{-1} in Figure 4 is in the region assigned to turn structures; bands at 1676 cm^{-1} (a transient absorption in Figure 4) have been assigned to either turn or extended chain conformations. The other main absorption at 1645 cm^{-1} is in the area assigned to unordered structure. Bands at lower frequency have been assigned to either β-sheet (Dong et al., 1990) or general β-type structures (Susi & Byler, 1986). In the case of Mb, the lower frequency signals would represent bleaching of the small regions of β-turns since the protein contains no β-sheet (Kuriyan et al., 1986; Takano, 1977). Assignments of the bands in the region below 1640 cm^{-1} are complicated by theoretical analyses which indicate that these bands can also arise from α-helix structures due to mixing of coupled vibrations (Surewicz et al., 1993; Torii & Tasumi, 1992). In order to make more specific structural assignments to each of the spectral features in Figure 4, additional data is required. However, it is clear that the major difference features at 1645, 1664, and 1676 cm^{-1} are due to changes in secondary structure involving the turn regions and some unordered structures. These assignments are consistent with the static differences between the crystal structures, which reveal that the helix structures of the CO and deoxy forms are essentially identical, but shift relative to each other (Kuriyan et al., 1986). These secondary structural changes apparently reflect the greater rigidity of the α-helical sections of the protein

than the corners (Seno & Go, 1990), such that the global displacement of the proximal helices is absorbed by the corners.

We conclude that the major IR difference features are due to changes in the polypeptide backbone conformation associated with the global relaxation of the proximal helices of the protein and that this relaxation is faster than the 100-ns time resolution of our instrument. These dynamics can be compared to previous, indirect measurements of the protein response to CO photodissociation. Resonance Raman measurements of the heme pocket relaxation indicate that the Fe–N(His) stretching frequency reaches its equilibrium deoxy value within the 30-ps (probe pulse width) time resolution of the experiment (Findsen et al., 1985). This result implies that local structural changes in the vicinity of the heme coupled to the position of the proximal histidine are complete within less than 30 ps. Another measure of the protein response to CO photodissociation was obtained from picosecond phase grating spectroscopy (Richard et al., 1992). These experiments suggest that a global change in the protein structure, sensed by the atomic displacements of the exterior of the protein, is occurring in less than 30 ps. Changes in the transient Soret absorption have been assigned to protein conformational relaxation (Ansari et al., 1992). In water, the large-amplitude absorbance changes assigned to the global protein motion are complete by the earliest times (10 ns) observable in these experiments; these dynamics are slowed to the microsecond time scale in water/glycerol mixtures at low temperatures due to increased solvent viscosity. Finally, picosecond IR experiments in our laboratories indicate that some of the difference features of Figure 4 are fully developed within 15 ps (Causgrove & Dyer, 1993b). All of these results are consistent with protein relaxation occurring on a picosecond time scale. Our results indicate that the nature of this relaxation is the change in polypeptide backbone conformation which accompanies the movement of the proximal histidine and the global displacement of the protein atoms on the proximal side of the heme.

Slow processes (relative to the global relaxation) attributed to protein relaxation have also been observed in previous spectroscopic measurements. A 700-ns process observed in water at 20 °C by photoacoustic calorimetry (Westrick et al., 1990) has been attributed to the breaking of a salt bridge. A small amplitude change in the Soret absorbance occurs on a similar time scale and has been postulated to be the same process (Ansari et al., 1992). Relaxation of the transient circular dichroism spectrum probed at 355 nm (the near-UV CD spectrum of proteins is generally dominated by contributions of aromatic side chains) of photodissociated MbCO to the equilibrium deoxy spectrum requires 300 ps (Xie & Simon, 1991). All of these slower processes appear to involve motions of specific side chains, probably on the distal side of the heme. No such slow transients are observed in our measurements, most likely because the spectral region probed is dominated by contributions from amide I (the polypeptide backbone).

In conclusion, we have shown that TRIR provides a structure-specific method for following the dynamics of conformational changes as a consequence of protein function. TRIR difference features for Mb are assigned to the changes in protein secondary structure associated with the global relaxation of the proximal protein helices following CO photodissociation. The dynamics of this process are faster than the 100-ns time resolution of the experiment. No protein dynamics were observed which could be definitively assigned to the formation of pathways and ligand diffusion through the protein. Future studies will focus on identifying side-chain vibrations, particularly those which may be associated with the transient structures which form the pathway into and out of the heme pocket. Further information on the assignment of the infrared difference features could be gained from perturbed systems. For example, the contribution of some ionizable side chains is in principle available from pH-dependent studies; other side-chain vibrations can be addressed through selective isotopic labeling and site-directed mutagenesis. Finally, the TRIR approach developed to study myoglobin functional dynamics is generally applicable to all protein dynamics that can be photo-initiated (e.g., by laser-induced pH and T-jumps as well as by photochemistry).

ACKNOWLEDGMENT

We thank Drs. Joel Berendzen and Hans Frauenfelder for helpful discussions and Dr. Doug Lemon for help in preparing the samples.

REFERENCES

Anfinrud, P. A., Han, C., & Hochstrasser, R. M. (1989) *Proc. Natl. Acad. Sci. U.S.A. 86,* 8387–8391.

Ansari, A., Jones, C. M., Henry, E. R., Hofrichter, J., & Eaton, W. A. (1992) *Science 256,* 1796–1798.

Case, D. A., & Karplus, M. (1979) *J. Mol. Biol. 132,* 343–68.

Causgrove, T. P., & Dyer, R. B. (1993a) *Proc. SPIE-Int. Soc. Opt. Eng. 1890* (in press).

Causgrove, T. P., & Dyer, R. B. (1993b) in *Proceedings of the 6th International Conference on Time-Resolved Vibrational Spectroscopy* (Lau, A., & Siebert, F., Eds.) Springer-Verlag, Berlin (in press).

Chirgadze, Y. N., Fedorov, O. V., & Trushina, N. P. (1975) *Biopolymers 14,* 679–694.

Diller, R., Iannone, M., Bogomolni, R., & Hochstrasser, R. M. (1991) *Biophys. J. 60,* 286–289.

Dixon, A. J., Glyn, P., Healy, M. A., Hodges, P. M., Jenkins, T., Poliakoff, M., & Turner, J. J. (1988) *Spectrochim. Acta 44A,* 1309–1314.

Dong, A., Huang, P., & Caughey, W. S. (1990) *Biochemistry 29,* 3303–3308.

Dong, A., Huang, P., & Caughey, W. S. (1992) *Biochemistry 31,* 182–189.

Dousseau, F., & Pézolet, M. (1990) *Biochemistry 29,* 8771–8779.

Dyer, R. B., Einarsdöttir, Ó., Killough, P. M., López-Garriga, J. J., & Woodruff, W. H. (1989) *J. Am. Chem. Soc. 111,* 7657–7659.

Elber, R., & Karplus, M. (1990) *J. Am. Chem. Soc. 112,* 9161–9175.

Elliott, A., & Ambrose, E. J. (1950) *Nature 165,* 921–922.

Findsen, E. W., Friedman, J. M., Ondrias, M. R., & Simon, S. R. (1985) *Science 229,* 661–665.

Frauenfelder, H., Sligar, S. G., & Wolynes, P. G. (1991) *Science 254,* 1598–603.

Gerwert, K., Rodriguez-Gonzalez, R., & Siebert, F. (1985) in *Time-resolved Vibrational Spectroscopy* (Laubereau, A., & Stockburger, M., Eds.) pp 263–268, Springer-Verlag, Berlin.

Gibson, Q. H. (1956) *J. Physiol. 136,* 112–122.

Gibson, Q. H., Olson, J. S., McKinnie, R. E., & Rohlfs, R. J. (1986) *J. Biol. Chem. 261,* 10228–10239.

Henry, E. R., Sommer, J. H., Hofrichter, J., & Eaton, W. A. (1983) *J. Mol. Biol. 166,* 443–451.

Jedju, T. M., Rothberg, L., & Labrie, A. (1988) *Opt. Lett. 13,* 961–963.

Kaiden, K., Matsui, T., & Tanaka, S. (1987) *Appl. Spectrosc. 41,* 180–184.

Kuriyan, J., Wilz, S., Karplus, M., & Petsko, G. A. (1986) *J. Mol. Biol. 192,* 133–154.

Lambright, D. G., Balasubramanian, S., & Boxer, S. G. (1989) *J. Mol. Biol. 207,* 289–299.

Martin, J.-L., Migus, A., Poyart, C., Lecarpentier, Y., Astier, R., & Antonetti, A. (1983) *Proc. Natl. Acad. Sci. U.S.A. 80,* 173–177.

Moore, J. N., Hansen, P. A., & Hochstrasser, R. M. (1987) *Chem. Phys. Lett. 138,* 110–114.

Nobbs, C. L. (1966) in *Hemes and Hemoproteins* (Chance, B., Eastbrook, R. W., & Yonetani, T., Eds.) pp 143–147, Academic Press, New York.

Perutz, M. F., Fermi, G., Luisi, B., Shannan, B., & Liddington, R. C. (1987) *Acc. Chem. Res. 20,* 309–321.

Powers, L., Chance, B., Chance, M., Campbell, B., Friedman, J., Khalid, S., Kumar, C., Naqui, A., Reddy, K. S., & Zhou, Y. (1987) *Biochemistry 26,* 4785–4796.

Richard, L., Genberg, L., Deak, J., Chiu, H.-L., & Miller, R. J. D. (1992) *Biochemistry 31,* 10703–10715.

Schlereth, D. D., & Mäntele, W. (1992) *Biochemistry 31,* 7494–7502.

Seno, Y., & Go, N. (1990) *J. Mol. Biol. 216,* 111.

Surewicz, W. K., & Mantsch, H. H. (1988) *Biochim. Biophys. Acta 952,* 115–130.

Surewicz, W. K., Mantsch, H. H., & Chapman, D. (1993) *Biochemistry 32,* 389–394.

Susi, H., & Byler, D. M. (1986) *Methods Enzymol. 130,* 291–311.

Takano, T. (1977) *J. Mol. Biol. 110,* 569–584.

Torii, H., & Tasumi, M. (1992) *J. Chem. Phys. 96,* 3379–3387.

Westrick, J. A., Peters, K. S., Ropp, J. D., & Sligar, S. (1990) *Biochemistry 29,* 6741–6746.

Xie, X., & Simon, J. D. (1991) *Biochemistry 30,* 3682–3692.